An investigation of the p-31 (d,p)p-32 reaction.

Piraino, Daniel.

Massachusetts Institute of Technology

AN INVESTIGATION OF THE $P^{31}(d,p)P^{32}$ REACTION

DANIEL PIRAINO

AN INVESTIGATION OF THE $P^{31}(d,p)P^{32}$ REACTION

by

Daniel Piraino

B. S., University of Idaho
(1951)

Submitted in Partial Fulfillment of the

Requirements for the Degree of

Master of Science

at the

MASSACHUSETTS INSTITUTE OF TECHNOLOGY

June 1958

AN INVESTIGATION OF THE $P^{31}(d,p)P^{32}$ REACTION

by

Daniel Piraino
Lieutenant, U. S. Navy

Submitted to the Department of Physics on May 26, 1958
in partial fulfillment of the requirements for the degree of

Master of Science

ABSTRACT

The MIT-ONR electrostatic accelerator and broad-range spectrograph have been employed to investigate the $P31(d,p)P32$ reaction. Thin targets of silver pyrophosphate evaporated onto Formvar films were bombarded with 6-Mev deuterons. The proton groups corresponding to excitation of the ground state of P^{32} and of the fifty-two excited levels were analyzed at laboratory angles of 30, 50, 70, and 90 degrees. The ground-state Q-value was found to be 5.709 ± 0.010 Mev in good agreement with results by other experimenters. Several levels, which were obscured by contaminant groups in the previous work on this nucleus, were identified, as well as many levels not previously resolved.

Because of the relatively large amounts of sodium in the evaporated material, it was possible to confirm the ground-state Q-value of the $Na^{23}(d,p)Na^{24}$ reaction. Proton groups corresponding to transitions to the ground state and nineteen excited levels in Na^{24} were found in this work.

Thesis Supervisor: W. W. Buechner

Title: Professor of Physics

ACKNOWLEDGMENTS

The author wishes to express his appreciation and thanks to the members of the High Voltage Laboratory for their assistance and cooperation, without which this work could not have been accomplished.

I am particularly indebted to Dr. C. H. Paris of the University of Utrecht for his guidance and instructions during the early part of the experimental work. Professor W. W. Buechner was a most helpful and patient adviser, as were Professor H. A. Enge, Mr. A. Sperduto, and Mr. M. Mazari of the University of Mexico.

I would like to thank Mr. Pieter Mimno for his help with the IBM calculation of Q-values, Mr. W. A. Tripp, Miss Estelle Freedman, Mrs. Mary Fotis, and Miss Sylvia Darrow for their patience in counting of tracks on the nuclear photographic plates; Mrs. Grace Rowe and Miss Sylvia Darrow for preparation of the drawings and charts in this thesis, and Mr. Everett W. Nickerson for his extensive aid and advice with mechanical problems.

Finally, I wish to thank Mrs. Mary E. White for the excellent preparation of the manuscript.

ACKNOWLEDGMENT

The author wishes to express his appreciation and thanks to the members of the High Voltage Laboratory for their assistance and cooperation, without which this work could not have been accomplished.

I am particularly indebted to Dr. G. B. Harris of the Battelle Memorial Institute for his guidance and instructions during the early part of the experimental work. Professor W. B. Lineweaver was a most helpful and patient adviser, as were Professor H. A. Erge, Mr. A. Jepsen, and Mr. K. Jones of the University of Wichita.

I would like to thank Mr. Foster Adams for his help with the IBM calculations of "values," Mr. W. A. Feiler, Miss Cecile Freeman, Mrs. Mary Fields, and Miss Sylvia Sawyer for their assistance in proofreading of these manuscripts for typographical errors. Thank you and Miss Sylvia Sawyer for preparation of the drawings and charts in this thesis, and Mr. Everett W. Patterson for his cooperative aid and advice with mechanical problems.

Finally, I wish to thank Mary K. White for the excellent preparation of the manuscript.

TABLE OF CONTENTS

TABLE OF CONTENTS

LIST OF ILLUSTRATIONS

LIST OF TABLES

LIST OF ILLUSTRATIONS

LIST OF TABLES

I. Introduction

The MIT-ONR electrostatic accelerator used in conjunction with the broad-range spectrograph is particularly well suited to the determination of nuclear energy levels. In this work, the equipment is used to determine the energy levels of P^{32} by analysis of the proton groups from the $P^{31}(d,p)P^{32}$ reaction.

According to the shell model[1], the nucleus P^{32} has a single proton hole in the $s_{1/2}$ shell and a single neutron in the $d_{3/2}$ shell. It is therefore amenable to treatment by the method of Goldstein and Talmi.[2] These authors have developed a set of equations for determining the binding energies of nuclei such as P^{32} in terms of various nuclear parameters, including the nuclear spins of the ground state and of the excited levels. To provide a check for these calculations, it is desirable to have information on the energy levels and spins of the levels in the nucleus. The energy levels are determined by methods described in this work. A limit can be set on the spins of the levels by employing the stripping theory of Butler.[3] Butler derives an expression for the cross section of the (d,p) reaction as a function of the reaction angle, with ℓ_n, the momentum of the captured neutron, as a parameter. By measuring the total number of particles at various angles in a proton group corresponding to a particular nuclear state, the experimental variation of reaction cross section can be determined. This is then compared with the theoretical curve from the Butler theory to determine the value of ℓ_n which gives the best fit to the data. In this way, limits can be set on the spin of the level in question in accordance with the relation[4]

I. Introduction

$$\text{min of } \left| \pm J_A \pm \ell_n \pm \tfrac{1}{2} \right| \leq J_B \leq J_A + \ell_n + \tfrac{1}{2}$$

where

J_A = spin of target nucleus

J_B = spin of residual nucleus

ℓ_n = angular momentum of captured neutron

As the first step in obtaining the necessary data, this work was aimed at identifying and measuring the energy of the excited states of P^{32} from an analysis of the $P^{31}(d,p)P^{32}$ reaction. An accurate Q-value for the ground-state transition is also obtained in this analysis.

[illegible] $\left| \vec{r} + \vec{q}_{\perp}' + q^{0} \frac{\vec{r}}{r} \right| = q'^{2} \leq \vec{r}^{2} + q^{0}{}^{2} + \beta$

where

$\vec{q}'$ = spin of target nucleus

q^{0} = spin of residual nucleus

β^{0} = angular momentum of captured neutron

As the first step in applying the necessary data, this work was aimed at theoretically and measuring the energy of the nuclear states of $_{32}Ge$ from an analysis of the $_{33}As^{75}(q^{0},\gamma)_{32}Ge^{76}$ reaction. An accurate formula for the crystal-state excitation is also obtained in this analysis.

II. Apparatus

This investigation was carried out using the MIT-ONR electrostatic accelerator and the associated deflecting magnet, collimating slit system, target chamber, and broad-range spectrograph.[5,6]

Analyzing Magnet

A cut-away drawing depicting the salient features of the accelerator is shown in Figure 1. The energy of the charged-particle beam and the spread in energy are defined by a collimating slit system and the deflecting magnet. The latter acts as a momentum filter. The momenta of particles which can pass through the magnet gap are determined by the setting of the magnetic field strength, which can be accurately measured as described below. The slit system controls the allowed energy spread in the incident beam, according to the relation[7]

$$R = \frac{a_o}{2\omega''} (M + 1)$$

where

R = energy resolution

a_o = radius of curvature of rays

$\omega'' = M\omega'$

ω' = width of entrance slit

M = magnification.

II. Apparatus

This investigation was carried out using the MIT-ONR electrostatic accelerator and the associated deflecting magnet, collimating slit system, Faraday cup, and Brown-recess electrometer.[3,4]

Analyzing System

A cut-away drawing depicting the optical features of the accelerator is shown in Figure 1. The energy of the accelerated beam and the current in energy are defined by a collimating slit system and the deflecting magnet. The latter acts as a momentum filter. The momenta of particles which can just pass through are determined by the setting of the magnetic field strength, which can be accurately measured as described below. The slit system then conducts the filtered energy sorted in the incident beam, according to the relation[3]

$$E = \frac{r^2}{2m} \quad (E = J)$$

where

E = energy constituted

r_0 = radius of curvature of path

r' = Ep

M = weight of monomeam unit

E = ionization.

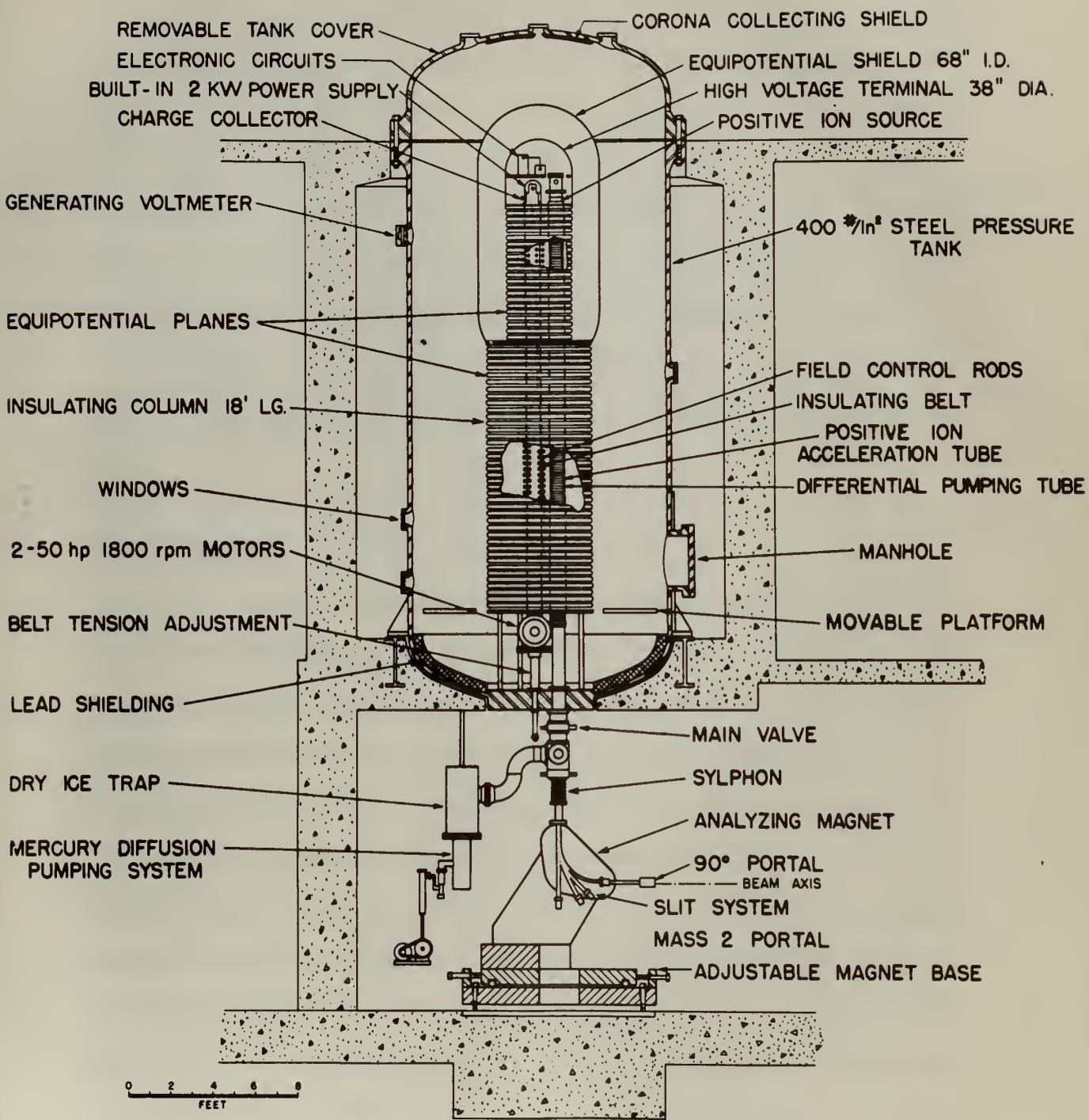
REMOVABLE TANK COVER
ELECTRONIC CIRCUITS
BUILT-IN 2 KW POWER SUPPLY
CHARGE COLLECTOR
GENERATING VOLTMETER
EQUIPOTENTIAL PLANES
INSULATING COLUMN 18' LG.
WINDOWS
2-50 hp 1800 rpm MOTORS
BELT TENSION ADJUSTMENT
LEAD SHIELDING
DRY ICE TRAP
MERCURY DIFFUSION PUMPING SYSTEM
CORONA COLLECTING SHIELD
EQUIPOTENTIAL SHIELD 68" I.D.
HIGH VOLTAGE TERMINAL 38" DIA.
POSITIVE ION SOURCE
400 #/in² STEEL PRESSURE TANK
FIELD CONTROL RODS
INSULATING BELT
POSITIVE ION ACCELERATION TUBE
DIFFERENTIAL PUMPING TUBE
MANHOLE
MOVABLE PLATFORM
MAIN VALVE
SYLPHON
ANALYZING MAGNET
90° PORTAL
BEAM AXIS
SLIT SYSTEM
MASS 2 PORTAL
ADJUSTABLE MAGNET BASE
0 2 4 6 8
FEET

Figure 1

For the magnet in use at M.I.T., $M \approx 0.6$, $a_o \approx 60$ cm, so that a slit width of 1 mm gives an energy resolution of about 1:800. The spread in the input energy is further controlled by a corona current stabilizer that uses a portion of the beam current to control the current to the terminal. After passing through the deflector magnet, where its direction is rotated through 90 degrees, the beam is focused on a set of defining slits placed 185 cm from the exit face of the magnet. The beam current collected on these insulated slit jaws is used to provide the corona current stabilization mentioned above.

Target Chamber

The particle beam next enters the target chamber in which are placed the thin targets to be bombarded. It has been observed that, when targets are exposed to a particle beam, contaminants, particularly carbon, build up on the surface of the target illuminated by the beam. This build-up causes a broadening of the output particle peaks because of energy straggling and introduces an error into the energy determinations. To minimize this effect and also to preclude fracturing of the fragile targets, the target frames are mounted in a rotating mechanism. This consists of a small D. C. motor mounted on the lid of the target chamber. A shaft is mounted eccentrically on the rotor, and this in turn holds the target frame. A circular motion of the target in a plane perpendicular to the incident beam

Target Chamber

is thus produced. This causes the beam spot to illuminate the target over a ring-shaped area on the target of mean diameter about 1 cm.

Broad-range Spectrograph

The particles emerging from the target chamber into the acceptance angle of the spectrograph (Figure 2) are deflected by the spectrograph's magnetic field with radii of curvature proportional to their momenta. Placed in the hyperbolic focal surface of the spectrograph are three 2 x 10-inch Eastman NTA 25-micron photographic plates that record the emergent particles. The plates are held rigidly in a specially contructed plateholder that constrains them to conform to the focal surface. Prior to loading in the spectrograph, the plates are indexed by shining light through a series of slits whose separations are very accurately known. These index marks serve as reference points for measuring distance along the plates when counting the particle tracks. The spectrograph can be rotated about a vertical axis through angles from zero to 130 degrees with respect to the direction of the incident beam. The angle of observation can be determined with an error of less than 10 minutes of arc. The solid angle of the spectrograph is independent of the angle of observation for the usual setting of the collimating slits. It is defined by an entrance aperture and by an 8 mm slit in front of the focal surface. The aperture angle is adjustable, but is normally used with a half angle of $2\frac{1}{2}$ degrees. The solid angle on the

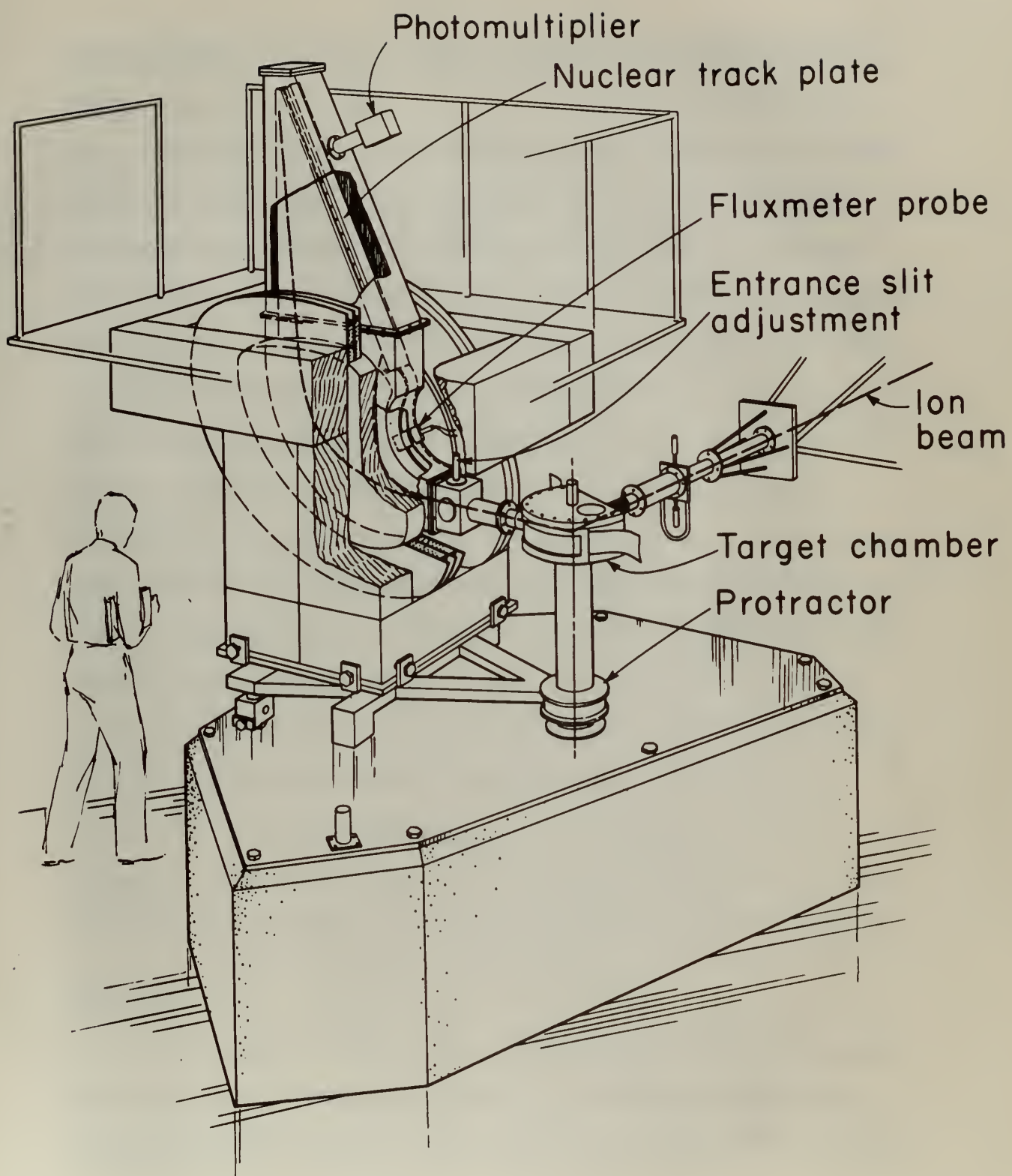
Photomultiplier
Nuclear track plate
Fluxmeter probe
Entrance slit adjustment
Ion beam
Target chamber
Protractor

Figure 2

focal surface is about 3.4×10^{-4} steradians at a plate distance of 52 cm.

In order to have a correlation between the position of charged-particle groups along the photographic plate and their momentum, it is necessary to calibrate the spectrograph with a known standard. Alpha particles from the radioactive isotope Po^{210} (RaF) are used for this purpose. A silver wire is coated with a thin layer of polonium by dipping it into a solution of a polonium salt for about 10 minutes. The wire is then placed in the target chamber, and its position is fixed to correspond with the position of the beam spot from the accelerator. The alpha particles are allowed to enter the spectrograph where they are deflected onto the photographic plates. This is done for various values of the spectrograph magnetic field strength. The distances along the plate at which the one-third height of the alpha-particle groups is found are then plotted against their radii of curvature, as determined by the known value of their momenta ($B\rho$ = 331.59 kilogauss-centimeters) and the magnetic induction B. The validity of using the distance to the one-third height on the high-energy side of the peak is discussed in detail by Buechner et al.[8]

Fluxmeters

The magnetic fields in the deflector and spectrograph magnets are measured and continuously monitored by fluxmeters employing a nuclear magnetic resonance technique. An aqueous solution of lithium

Timemeters

chloride contained in a small glass capsule is positioned between the pole faces of the magnet. The lithium nuclei will precess in the magnetic field with Larmor frequency

$$\nu = \frac{\mu_z H}{I h}$$

where

μ_z = the component of magnetic moment along H

H = magnetic field intensity

I = angular momentum of nucleus

h = Planck's constant.

A radio-frequency field of frequency F is applied to the capsule with its magnetic vector at right angles to H. At the resonance frequency F = ν, changes occur in the orientation of the nuclear moments corresponding to transitions between the magnetic substates in accordance with the relation[9]

$$E = m_I h\nu$$

where

m_I = I cos β is the magnetic quantum number for the projection of I along H

E = kinetic energy of Larmor precession.

This absorption of energy by the lithium nuclei causes a relatively large depression of the amplitude of the radio-frequency

signal applied to the capsule. This signal is applied to the vertical deflection plates of a cathode-ray oscilloscope. The damping of the signal at resonance is observed as a depression of the sweep on the face of the oscilloscope, and the magnet current is adjusted to keep the "pip" centered. This procedure allows the field strength to be determined to within the accuracy of measurement of the radio-frequency. The latter can be measured with an accuracy of 1 part in 100,000. A secondary frequency standard, which is checked periodically with station WWV, is used to determine the frequency accurately.

Alterations

During the period covered by this investigation, several changes were made in the accelerator. These were aimed at increasing the maximum operating voltage and beam current attainable.

The thyrites, which had been used to distribute the voltage along the length of the column, were replaced with resistors. These thyrites served to maintain a uniform voltage gradient throughout the length of the accelerator column. However, the thyrites originally installed for this purpose had a nonlinear characteristic such that the voltage across them saturated at a predetermined value of current. Therefore, based on previous experience and also on the experiences reported by other Van de Graaff groups, it was decided to install a linear resistor manufactured by the S. S. White Dental Manufacturing Company. This change resulted in several problems.

The first of these was the effect of ionization of the nitrogen gas used to insulate the generator. This ionization was caused by x-rays produced by electrons accelerated up the accelerator tube and stopped near the positive ion source at the top of the tube. This ionization caused a lowering of the potential of the intermediate shell, since the ion current from this shell to the walls of the tank was greater than that from the terminal to the shell because of the larger volume of gas involved. In attempting to bring the voltage back up, excessive charging currents were required on the accelerator belt, and this led to instability of the generator. The situation was remedied by construction of a 2-inch thick lead shield surrounding the ion source. This shield effectively attenuated the radiation produced by electron loading and thereby sufficiently reduced the ionization currents.

A second effect noted was the difficulty of stabilizing the generator voltage. The stabilizer presently in use controls the corona current to the intermediate shell which is connected to an equipotential plane two-thirds of the distance from the lower end of the generator. Present plans call for removal of this shell so that the stabilizer can control corona current to the terminal and thus have a stronger effect on the total generator voltage.

Target Preparation

The targets used in this work were prepared by evaporation of silver pyrophosphate onto thin Formvar films held on copper frames. The evaporation was carried out in a vacuum of about 10^{-3} mm of mercury. The material to be evaporated was carefully weighed (100 milligrams was used) and placed in a tantalum boat, which was heated by the passage of an electric current. The silver pyrophosphate evaporated from the boat and subsequently condensed onto the Formvar films that were placed at distances of 2 to 6 inches from the boat. The targets were of the order of 5- to 10-kev thick for 6-Mev incident deuterons. This thickness was determined by use of an alpha-particle thickness gauge[10] which measures the thickness in terms of an equivalent thickness of air. This figure can then be used to determine the thickness in terms of energy loss of incident particles.

III. Experimental Procedure

The Q-Equation

The type of reaction studied in this work is illustrated in Figure 3 (laboratory system).

The laws of conservation of energy and momentum require

$$E_1 + Q = E_R + E_0 \tag{1}$$

$$\vec{P}_1 = \vec{P}_0 + \vec{P}_R \tag{2}$$

where the E's and P's are kinetic energy and momentum, respectively. Using the conservation relations and solving the momentum triangle[11] it is found that

$$E_R = \frac{M_1}{M_R} E_1 + \frac{M_0}{M_R} E_0 - 2 \cos\theta \frac{\sqrt{M_1 M_0}}{M_R} \sqrt{E_1 E_0} + \delta_{rel} \tag{3}$$

where

$$\delta_{rel} \approx \frac{1}{2M_R c^2} \left(E_1^2 + E_0^2 - E_R^2 - \cos\theta \sqrt{M_1 M_0} \sqrt{E_1 E_0} \left(\frac{E_1}{M_1} + \frac{E_0}{M_0} \right) \right) \tag{4}$$

This equation contains E_R but sufficient accuracy is obtained if the nonrelativistic expression is used:

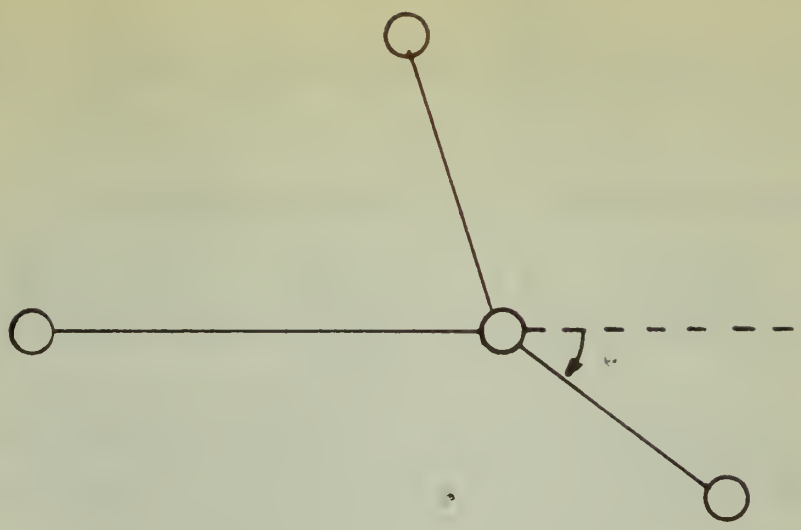

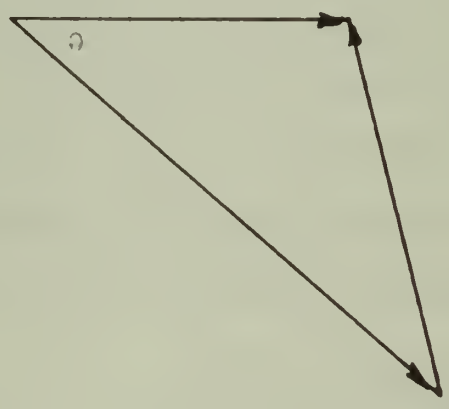

$$E_R = \frac{M_1}{M_R} E_1 + \frac{M_0}{M_R} E_0 - 2 \cos\theta \frac{\sqrt{M_1 M_0}}{M_R} \sqrt{E_1 E_0} \qquad (5)$$

Combining (1) and (4), the following equation is obtained:

$$Q = \frac{M_R + M_0}{M_R} E_0 - \frac{M_R - M_1}{M_R} E_1 - 2 \cos\theta \frac{\sqrt{M_1 M_0}}{M_R} \sqrt{E_1 E_0} + \delta_{rel.} \qquad (6)$$

This equation expresses Q in terms of the energies of the incident and output particles, which can be measured in each experiment.

To obtain the Q-value corresponding to the distance along the plate to the one-third height of each proton group, the following procedure is employed. The radius of curvature (ρ) of the particle, corresponding to this distance, is obtained from the calibration curve described above. This is multiplied by the magnetic induction (B) measured by the fluxmeter to give the momenta $B\rho$ of the particles. The relationship between $B\rho$ and energy is[11]

$$E = m_0 c^2 \left[\sqrt{1 + \left(\frac{ZeB\rho}{m_0 c}\right)^2} - 1 \right]$$

where

m_0 = electron mass

c = velocity of light

Z = charge of particle in units of electronic charge

B = magnet induction

ρ = radius of curvature

e = electronic charge

$$\beta = \frac{\beta_0}{\beta_0} \beta_0 + \frac{\beta_0}{\beta_0} \beta_0 \pm \cos \alpha \frac{\beta_0}{\beta_0} \sqrt{\beta_0 \beta_0} \sqrt{\beta_0 \beta_0} \qquad (3)$$

Combining (1) and (2), the following equation is obtained:

$$\beta = \frac{\beta_0 + \beta_0}{\beta_0} \beta_0 - \frac{\beta_0 - \beta_0}{\beta_0} \left[1 - 2 \cos \alpha \sqrt{\frac{\beta_0 \beta_0}{\beta_0 \beta_0}} \sqrt{\beta_0 \beta_0} + \beta^2 \right]^{\frac{1}{2}} \qquad (4)$$

This equation expresses β in terms of the curvature of the incident and output particles, which can be measured in each experiment.

To obtain the β-value corresponding to the distance along the plate to the one-third height of each proton group, the following procedure is employed. The radius of curvature (ρ) of the particle, corresponding to this distance, is obtained from the calibration curve described above. This is multiplied by the magnetic induction (B) measured by the fluxmeter to give the momenta (p) of the particles. The relationship between p and energy is[2]

$$\beta = \beta_0 c \left[1 - \left(\frac{\beta_0 c}{\beta_0 c} \right)^2 \right]^{\frac{1}{2}}$$

where

β_0 = electron mass

c = velocity of light

β = charge of particle in units of electronic charge

B = applied induction

ρ = radius of curvature

β = electronic energy

This equation may be expanded in powers of $(B\rho)^2$. The energies of protons, deuterons, tritons, and alpha particles have been tabulated by Enge[11] for values of $B\rho$ from 10^5 to 6.5×10^5 gauss centimeters. Using the value of input energy determined by elastic scattering and the output energy determined as described here, one can calculate the Q-value for each level. The calculations were greatly facilitated through the efforts of Mr. Pieter Mimno, who programmed this calculation for the IBM 704 computer at M.I.T. The results were presented as a table of Q-values for each centimeter of plate distance. Linear interpolation was used to find the Q-value corresponding to each proton group.

Target Mass Analysis

In preparation for exposing the targets to the deuteron beam, it is essential to know the relative abundance of target nuclei and contaminants. This information is useful as an aid in assigning the proton groups observed in the analysis of the (d,p) reaction to the proper reaction. Mass analysis of the target is accomplished by elastically scattering incident protons from the target and analyzing the scattered protons with the broad-range spectrograph. Because each nucleus will absorb momentum from the incident beam in inverse proportion to its mass, it is possible to identify a proton group with the mass of the scattering nucleus. From the Q-equation with Q set equal to zero for elastic scattering, we obtain, ignoring the small relativistic correction δ_{rel}:

$$m = \frac{m_p(E_0 + E_1) + 2\cos\theta\, m_p \sqrt{E_1 E_0}}{E_0 - E_1}$$

Where

m = mass of scattering nucleus

m_p = mass of proton

E_0 = energy of scattered proton

E_1 = energy of incident proton

θ = observation angle (laboratory system).

Figure 4 shows the results of a scattering mass analysis performed on the target used in this work. A beam of 6.03-Mev protons was used, and the scattered particles were analyzed at a reaction angle of 130 degrees. The elements present in the target can be attributed to the following:

Tantalum = boat material used in evaporation

Silver = evaporated material ($Ag_4P_2O_7$)

Phosphorus = evaporated material

Sodium = contaminant in evaporated material

Oxygen = Formvar backing; evaporated material

Nitrogen = Formvar backing; contaminant in evaporated material

Carbon = Formvar backing

Chlorine, silicon, and potassium = materials previously evaporated and not completely purged from system; contaminants in evaporated material.

$$\varepsilon = \frac{E_p\rho_0 + \Sigma_f) + \xi \nu\sigma_f \Lambda E_f\rho_0}{E_0 - \Sigma_f}$$

where

k = ratio of reproduction neutrons

E_f^0 = ratio of fission

E_p^0 = energy of captured in plan

Σ_f = energy of fissioned neutron

Ψ = observation angle (laboratory system).

Figure 4 shows the results of a calculation made analyzed
performed on the Burpee vacuum tin thin wall. A beam of σ.03-inch
neutrons was used, and the scattered particles were analyzed at a
reaction angle of 120 degrees. The elements present in the target
can be substituted to the following:

Tantalum = high molecular weight to evaporation

Silver = evaporated material (Ag^{107})

Beryllium = evaporated material

Sodium = carbonated to evaporated material

Oxygen = thinner backing) evaporated material

Nitrogen = thinner backing) contributed to evaporated
material

Carbon = thinner backing

Chlorine, silicon and potassium - materials involved
evaporated and not essentially merged them

systems contributed to evaporated material.

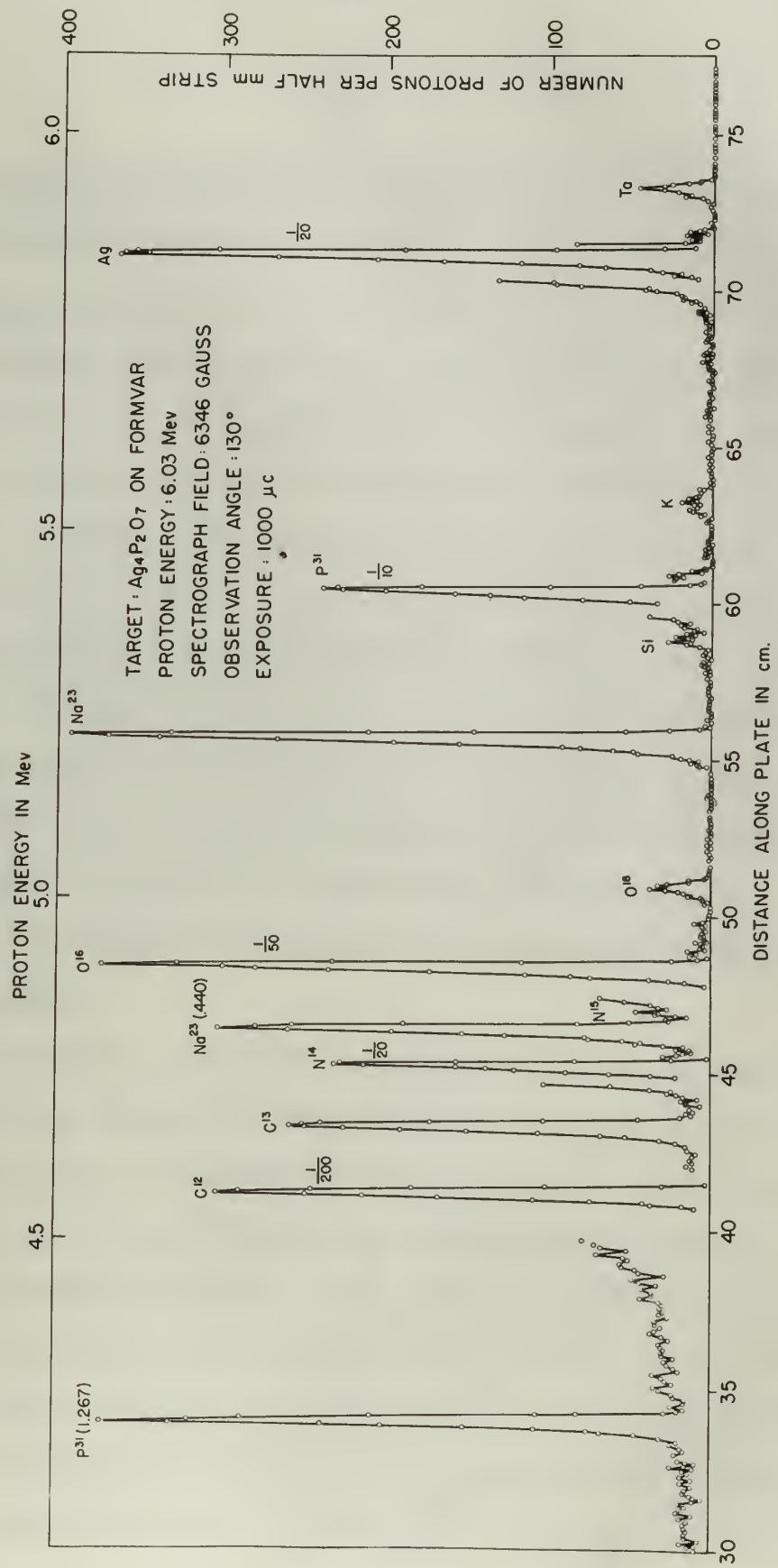
TARGET: $Ag_4P_2O_7$ ON FORMVAR
PROTON ENERGY: 6.03 Mev
SPECTROGRAPH FIELD: 6346 GAUSS
OBSERVATION ANGLE: 130°
EXPOSURE: 1000 μc
PROTON ENERGY IN Mev
DISTANCE ALONG PLATE IN cm.
NUMBER OF PROTONS PER HALF mm STRIP
P^{31}(1.267)
C^{12}
C^{13}
N^{14}
Na^{23}(440)
O^{16}
N^{15}
O^{18}
Na^{23}
Si
P^{31}
K
Ag
Ta
1/200
1/20
1/50
1/10
1/20

Figure 4.

The unusually high concentrations of sodium and nitrogen can be explained by noting the procedure for synthesizing silver pyrophosphate. This consists of combining silver nitrate and sodium pyrophosphate, which could explain the presence of these impurities. Inquiries at all leading chemical supply firms failed to produce a source of this compound with a high degree of purity. Attempts were made to evaporate metallic phosphates, which are available with a high degree of purity. It was found that it was not possible to get sufficient amounts of phosphorus nuclei onto the target, even with targets of 15-kev thickness. In particular, lead phosphate and cadmium phosphate were evaporated. A mass analysis of these targets showed large amounts of the metallic nuclei but extremely small quantities of phosphorus. Further study of this phenomenon is indicated to determine what happens to the phosphorus in the evaporation process.

Although the amounts of contaminant nuclei in the target were significantly higher than can normally be tolerated, it was decided to proceed with the analysis of the (d,p) reaction. The contaminant elements that would be expected to give appreciable yields are carbon, nitrogen, oxygen, and sodium. Since these elements have all been previously studied in this laboratory, it was felt that no difficulty would be experienced in picking out the proton groups from these contaminants. It is possible to distinguish unambiguously the proton groups ascribed to the $P^{31}(d,p)P^{32}$ reaction from the proton

groups arising from the contaminant elements by noting the relative shift in proton energy as a function of observation angle.

The (d,p) Reaction

A deuteron beam of 6.01 Mev was used to bombard the target. The energy of the incident deuterons was determined by measuring the energy of the deuterons elastically scattered from the phosphorus. Solving the Q- equation for E_1, we obtain:

$$E_1 = \frac{M_R + M_0}{M_R - M_1} E_0 - \frac{2 \cos\theta \sqrt{M_1 M_0 E_0 E_1}}{M_R - M_1} + \delta_{rel} \frac{M_R}{M_R - M_1}$$

This equation can be solved by successive approximations for E_1 in terms of the energy of the scattered deuterons.

The following exposures were used at the various angles of observation:

30 degrees - 500 μc

50 degrees - 1500 μc

70 degrees - 1000 μc

90 degrees - 1000 μc

The charged-particle beam , which is incident on the target, is measured and integrated by a combined sensitive microammeter and current integrater designed by Enge.[12] A 300-volt bias is employed in the target chamber to obviate the possibility of measuring false currents produced by secondary electrons. An additional expo-

$$T_1 = \frac{m_p + m_\alpha}{m_p - m_1} T_0 - \frac{2 \cos\phi \sqrt{T_0 (T_0 + 2m_p c^2)}}{m_p - m_1} + Q \frac{m_\alpha}{m_p - m_1}$$

sure of one-tenth the above values was made at each angle in order that the more intense proton groups, particularly those from carbon and oxygen, could be counted. Since the Q-values for the $C^{12}(d,p)C^{13}$ and $O^{16}(d,p)O^{17}$ reactions are well known, these groups serve as a good check on the input energy and also on the spectrograph field settings.

A typical spectrum of the proton groups is shown in Figure 5. It is noted that some of the groups are not resolved from contaminant groups, but these were all observed on at least one other exposure at a different observation angle where the relative shift in proton energy was sufficient to allow resolution of the phosphorus groups from those that were due to contaminants.

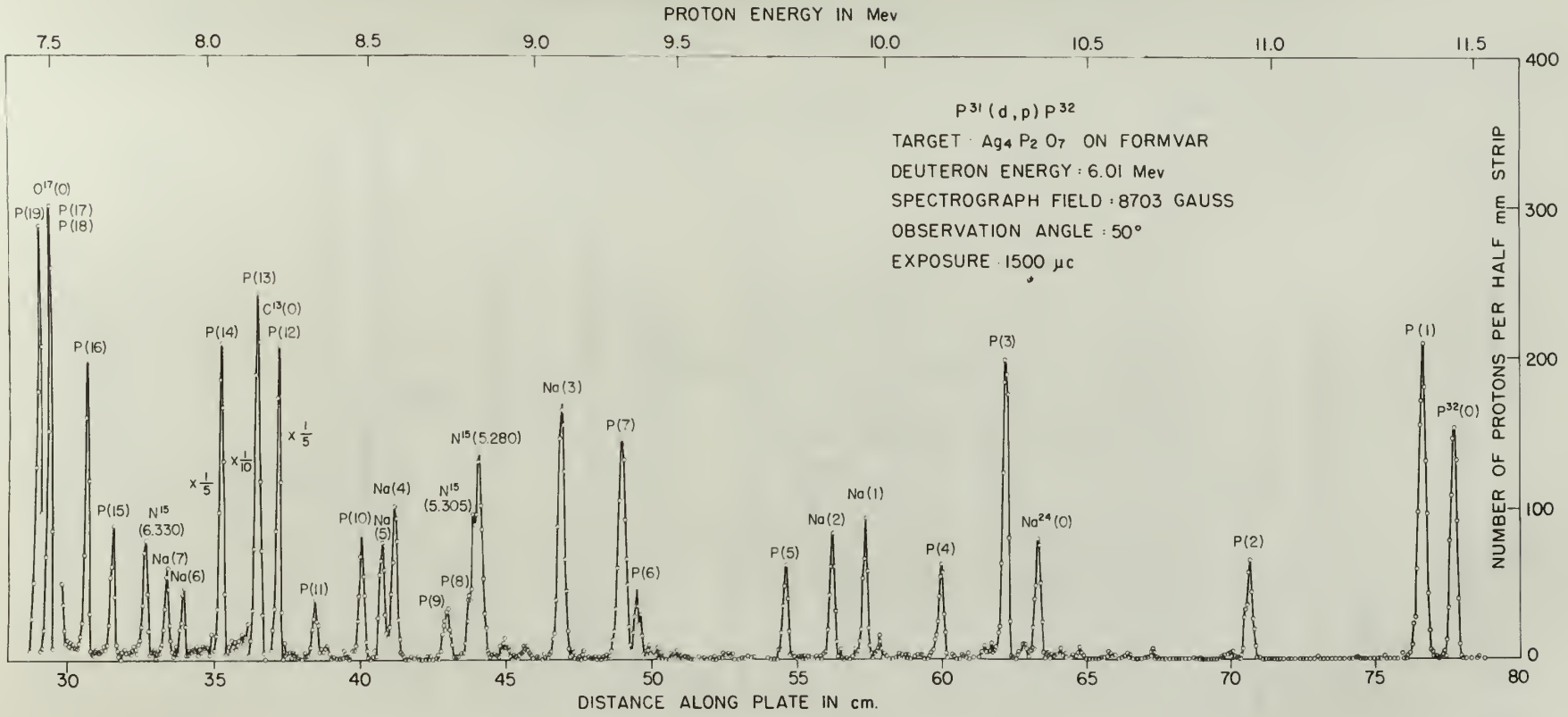
PROTON ENERGY IN Mev
7.5
8.0
8.5
9.0
9.5
10.0
10.5
11.0
11.5
P31 (d, p) P32
TARGET · Ag4 P2 O7 ON FORMVAR
DEUTERON ENERGY : 6.01 Mev
SPECTROGRAPH FIELD : 8703 GAUSS
OBSERVATION ANGLE : 50°
EXPOSURE · 1500 μc
O17(0)
P(19)
P(17)
P(18)
P(16)
P(15)
N15 (6.330)
Na(7)
Na(6)
P(14)
P(13)
C13(0)
P(12)
P(11)
P(10)
Na(5)
Na(4)
P(9)
P(8)
N15 (5.280)
N15 (5.305)
Na(3)
P(7)
P(6)
P(5)
Na(2)
Na(1)
P(4)
P(3)
Na24(0)
P(2)
P(1)
P32(0)
x 1/5
x 1/10
x 1/5
400
300
200
100
0
NUMBER OF PROTONS PER HALF mm STRIP
30
35
40
45
50
55
60
65
70
75
80
DISTANCE ALONG PLATE IN cm.

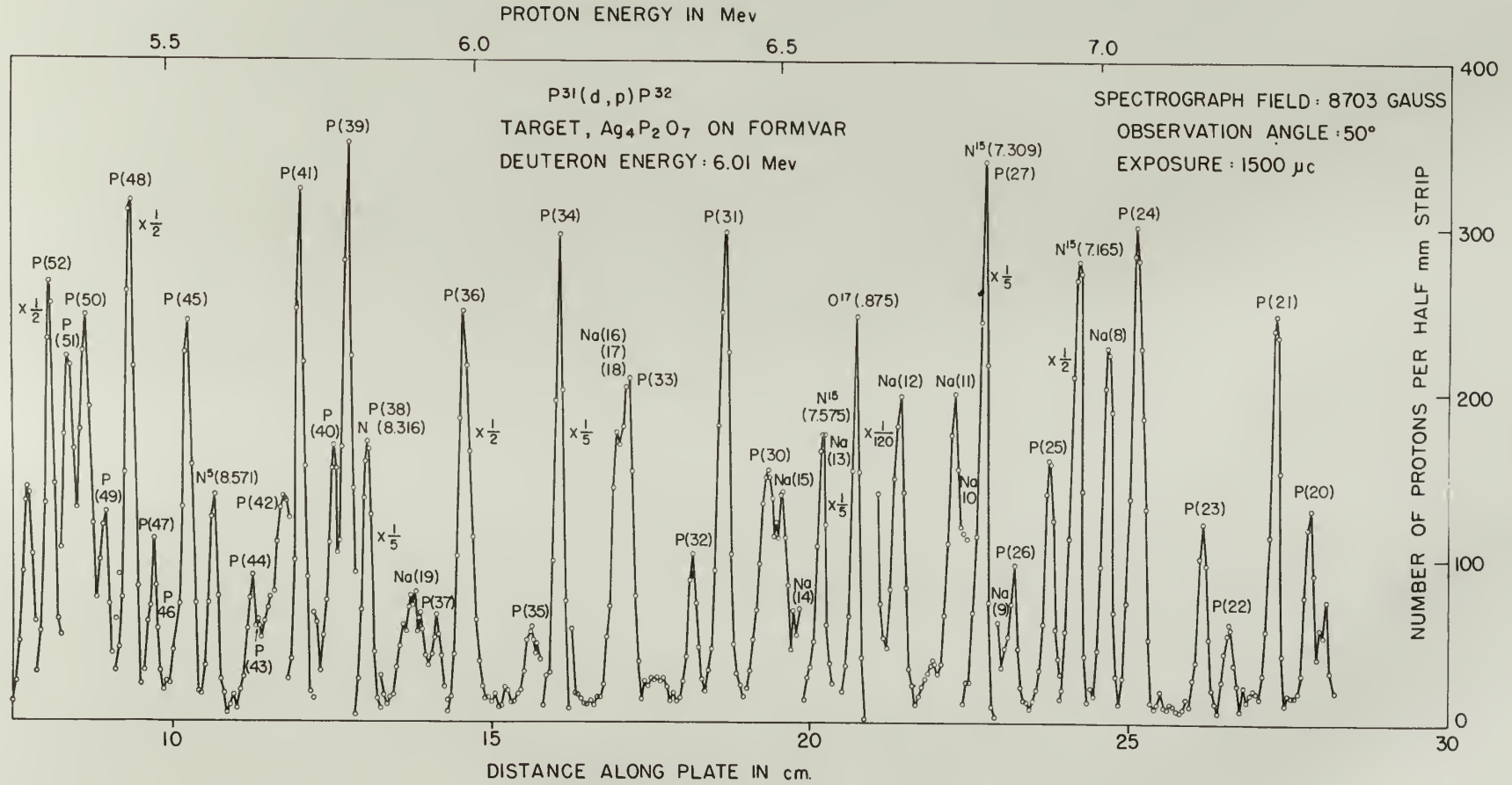
PROTON ENERGY IN Mev
5.5
6.0
6.5
7.0
P31(d,p)P32
TARGET, Ag4P2O7 ON FORMVAR
DEUTERON ENERGY: 6.01 Mev
SPECTROGRAPH FIELD: 8703 GAUSS
OBSERVATION ANGLE: 50°
EXPOSURE: 1500 μc
P(52)
P(50)
P(51)
P(48)
P(49)
P(47)
P46
P(45)
N5(8.571)
P(44)
P(43)
P(42)
P(41)
P(40)
P(39)
N (8.316)
P(38)
Na(19)
P(37)
P(36)
P(35)
P(34)
Na(16)
(17)
(18)
P(33)
P(32)
P(31)
P(30)
Na(15)
Na
(14)
N15
(7.575)
Na
(13)
O17(.875)
Na(12)
Na(11)
Na
10
N15(7.309)
P(27)
P(26)
Na
(9)
N15(7.165)
P(25)
Na(8)
P(24)
P(23)
P(22)
P(21)
P(20)
10
15
20
25
30
DISTANCE ALONG PLATE IN cm.
NUMBER OF PROTONS PER HALF mm STRIP
400
300
200
100
0

IV. Results

The $P^{31}(d,p)P^{32}$ Reaction

The ground-state Q-value for the $P^{31}(d,p)P^{32}$ reaction was determined as 5.709 ± 0.010 Mev, which agrees within the stated errors with the value of 5.704 ± 0.003 Mev reported by Van Patter et al.[13] Moreover, fifty-two proton groups were assigned to excited levels in P^{32} by virtue of their energy shift with observation angle. The results are summarized in Table I and Figure 6. The results of Van Patter et al, and those of Dalton et al.[14] are included for purposes of comparison. It is seen that agreement of the present work with that previously reported is quite good.

The $Na^{23}(d,p)Na^{24}$ Reaction

Sufficient yield was obtained from the $Na^{23}(d,p)Na^{24}$ reaction so that these results can also be presented for comparison with the work of Sperduto and Buechner.[15] A ground-state Q-value of 4.731 ± 0.010 Mev was found for the $Na^{23}(d,p)Na^{24}$ reaction in exact agreement with previous results. All nineteen of the excited levels reported earlier were confirmed in this investigation. These results are presented in Table II. It is somewhat surprising that there were no proton groups beyond the one corresponding to the 4.56-Mev level in Na^{24} which could be assigned to Na^{24}. It is probable that relatively weak sodium groups in this region may have been obscured at all observation angles by other more intense groups from P^{32} and

IV. Results

The $p_{32}(q,p)p_{36}$ Reaction

The ground-state Q-value for the $p_{32}(q,p)p_{36}$ reaction was determined as 5.109 ± 0.010 Mev, which agrees within the quoted errors with the value of 5.108 ± 0.008 Mev reported by Van Patter et al.[13] Moreover, fifty-two proton groups were analyzed to obtain levels in p_{36} by virtue of their energy shift with observation angle. The results are summarized in Table I and Figure 6. The results of Van Patter et al. and those of Dutton et al.[14] were included for purpose of comparison. It is seen that agreement of the present work with that previously reported is quite good.

The $Mg_{25}(q,p)Mg_{28}$ Reaction

Excitation yield was obtained from the $Mg_{25}(q,p)Mg_{28}$ reaction so that these results can also be presented for consideration with the work of Cerutto and Moscowitz.[15] A ground-state Q-value of 6.733 ± 0.010 Mev was found for the $Mg_{25}(q,p)Mg_{28}$ reaction to agree-ment with previous results. All members of the excited levels reported earlier were confirmed in this investigation. These results are presented in Table II. It is somewhat surprising that there were no proton groups observed to the 1.61-Mev level in Mg_{28} which could be assigned to Mg_{26}. It is possible that relatively weak proton groups in this region may have been obscured at all observation angles by other more intense proton groups from p_{36} and

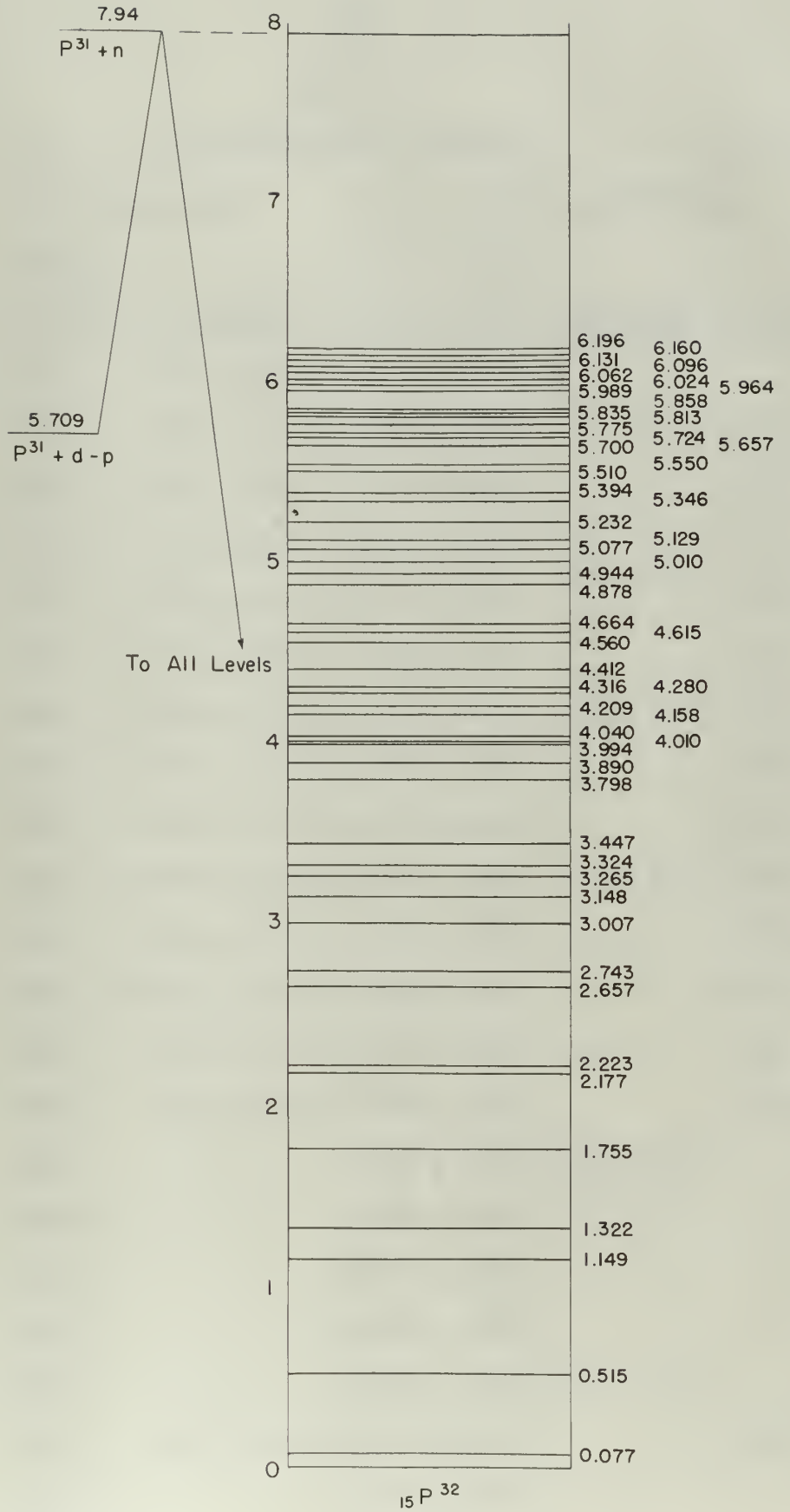
7.94
P31 + n
5.709
P31 + d - p
To All Levels
8
7
6
5
4
3
2
1
0
6.196
6.160
6.131
6.096
6.062
6.024
5.964
5.989
5.858
5.835
5.813
5.775
5.724
5.657
5.700
5.550
5.510
5.394
5.346
5.232
5.129
5.077
5.010
4.944
4.878
4.664
4.615
4.560
4.412
4.316
4.280
4.209
4.158
4.040
4.010
3.994
3.890
3.798
3.447
3.324
3.265
3.148
3.007
2.743
2.657
2.223
2.177
1.755
1.322
1.149
0.515
0.077
15P32

Table I

The $P^{31}(d,p)P^{32}$ Reaction

	Q-Value (Mev)		Levels in P^{32} (Mev)		
Level	Present Work ± 0.010	Van Patter[13]	Present Work	Dalton[14]	Van Patter[13]
0	5.709	5.704 ± 0.003	0	0	0
1	5.632	5.627 ± 0.003	0.077 ± 0.003		0.077 ± 0.002
2	5.193	5.189 ± 0.010	0.516 ± 0.003		0.515 ± 0.005
3	4.560	4.550 ± 0.007	1.149 ± 0.003		1.154 ± 0.007
4	4.387	4.388 ± 0.007	1.322 ± 0.003		1.316 ± 0.008
5	3.954	3.954 ± 0.007	1.755 ± 0.004		1.750 ± 0.009
6	3.532	3.527 ± 0.008	2.177 ± 0.004		2.177 ± 0.009
7	3.486	3.477 ± 0.008	2.223 ± 0.004		2.227 ± 0.009
8	3.052	3.054 ± 0.006	2.657 ± 0.005		2.650 ± 0.008
9	2.966	2.962 ± 0.006	2.743 ± 0.005		2.742 ± 0.008
10	2.702	2.705 ± 0.008	3.007 ± 0.005		2.999 ± 0.010
11	2.561	(2.563 ± 0.010)	3.148 ± 0.005		(3.141 ± 0.012)
12	2.444	2.445 ± 0.006	3.265 ± 0.005		3.259 ± 0.009
13	2.385	2.386 ± 0.006	3.324 ± 0.005		3.318 ± 0.009
14	2.262		3.447 ± 0.005	3.45 ± 0.10	
15	1.911		3.798 ± 0.006		
16	1.819		3.890 ± 0.006		
17	1.715		3.994 ± 0.006		
18	1.699		4.010 ± 0.006		
19	1.669	1.672 ± 0.005	4.040 ± 0.006		4.032 ± 0.009
20	1.551		4.158 ± 0.006		

Table I

The $^{32}S(\alpha,p)^{35}Cl$ Reaction

Level	Present Work ± 0.020	Van Patter[13]	Present Work	Endt[14]	Van Patter[13]
	Q-Value (MeV)		Levels in ^{35}Cl (MeV)		
0	5.709	5.708 ± 0.004	0	0	0
1	5.532	5.527 ± 0.004	0.177 ± 0.002		0.177 ± 0.002
2	5.193	5.189 ± 0.010	0.516 ± 0.002		0.515 ± 0.005
3	4.560	4.550 ± 0.007	1.149 ± 0.002		1.158 ± 0.007
4	4.347	4.348 ± 0.007	1.362 ± 0.002		1.376 ± 0.008
5	3.954	3.954 ± 0.007	1.755 ± 0.004		1.750 ± 0.009
6	3.532	3.527 ± 0.008	2.177 ± 0.004		2.177 ± 0.009
7	3.466	3.477 ± 0.008	2.223 ± 0.004		2.227 ± 0.009
8	3.082	3.034 ± 0.006	2.657 ± 0.003		2.650 ± 0.008
9	2.964	2.962 ± 0.008	2.743 ± 0.005		2.748 ± 0.008
10	2.702	2.702 ± 0.008	3.007 ± 0.006		2.999 ± 0.010
11	2.561	(2.503 ± 0.010)	3.140 ± 0.005		(3.148 ± 0.012)
12	2.444	2.446 ± 0.006	3.265 ± 0.005		3.259 ± 0.009
13	2.395	2.396 ± 0.006	3.314 ± 0.005		3.318 ± 0.009
14	2.262		3.447 ± 0.005	3.45 ± 0.10	
15	1.911		3.798 ± 0.006		
16	1.819		3.890 ± 0.006		
17	1.715		3.994 ± 0.006		
18	1.699		4.010 ± 0.006		
19	1.689	1.672 ± 0.005	4.040 ± 0.006		4.032 ± 0.009
20	1.551		4.159 ± 0.006		

21	1.499	1.497 ± 0.008	4.209 ± 0.006		4.207 ± 0.010
22	1.428		4.280 ± 0.006		
23	1.393		4.316 ± 0.006		
24	1.296		4.412 ± 0.006	4.43 ± 0.1	
25	1.149		4.560 ± 0.007		
26	1.094		4.615 ± 0.007		
27	1.045		4.664 ± 0.007		
28	0.831		4.878 ± 0.007	4.90 ± 0.07	
29	0.764		4.944 ± 0.007		
30	0.699		5.010 ± 0.007		
31	0.632		5.077 ± 0.007	5.11 ± 0.1	
32	0.580		5.129 ± 0.007		
33	0.476		5.232 ± 0.007		
34	0.362		5.346 ± 0.007	5.37 ± 0.07	
35	0.314		5.394 ± 0.007		
36	0.199		5.510 ± 0.006		
37	0.159		5.550 ± 0.008		
38	0.052		5.657 ± 0.008		
39	0.009		5.700 ± 0.008		
40	-0.016		5.724 ± 0.008	5.75 ± 0.1	
41	-0.067		5.775 ± 0.008		
42	-0.104		5.813 ± 0.008		
43	-0.126		5.835 ± 0.008	5.82 ± 0.07	
44	-0.150		5.858 ± 0.008		

21	1.499	1.497 ± 0.008	4.209 ± 0.008	4.307 ± 0.010
22	1.429		4.200 ± 0.004	
23	1.393		4.336 ± 0.004	
24	1.359		4.452 ± 0.004	4.49 ± 0.3
25	1.348		4.500 ± 0.007	
26	1.098		4.515 ± 0.007	
27	1.045		4.665 ± 0.007	
28	0.831		4.976 ± 0.007	
29	0.764		4.984 ± 0.007	4.80 ± 0.07
30	0.659		5.040 ± 0.007	
31	0.638		5.077 ± 0.007	5.33 ± 0.3
32	0.589		5.307 ± 0.007	
33	0.476		5.358 ± 0.007	
34	0.364		5.389 ± 0.007	5.37 ± 0.07
35	0.314		5.384 ± 0.007	
36	0.329		5.320 ± 0.004	
37	0.159		5.389 ± 0.008	
38	0.088		5.027 ± 0.004	
39	0.079		5.380 ± 0.008	
40	-0.016		5.126 ± 0.004	5.32 ± 0.3
41	-0.047		5.172 ± 0.004	
42	-0.308		5.253 ± 0.002	
43	-0.126		5.298 ± 0.004	5.42 ± 0.07
44	-0.329		5.402 ± 0.004	

45	-0.255	5.964 ± 0.008	
46	-0.280	5.989 ± 0.008	
47	-0.316	6.024 ± 0.008	
48	-0.354	6.062 ± 0.008	
49	-0.388	6.096 ± 0.008	6.09 ± 0.07
50	-0.422	6.131 ± 0.008	
51	-0.452	6.160 ± 0.008	
52	-0.487	6.196 ± 0.008	6.20 ± 0.1

12	-0.482	6.126 ± 0.020	6.30 ± 0.1
11	-0.422	6.260 ± 0.020	
10	-0.422	6.121 ± 0.020	
9	-0.388	6.056 ± 0.020	6.06 ± 0.02
8	-0.364	6.052 ± 0.020	
7	-0.346	6.060 ± 0.020	
6	-0.330	5.988 ± 0.020	
5	-0.252	5.968 ± 0.020	

Table II

The $Na^{23}(d,p)Na^{24}$ Reaction

	Q-Value (Mev)		Levels in Na^{24} (Mev)	
Level	Present Work ± 0.010	Sperduto and Buechner	Present Work	Sperduto and Buechner
0	4.731	4.731 ± 0.007	0	0
1	4.260	4.259 ± 0.007	0.471 ± 0.003	0.472 ± 0.008
2	4.169	4.167 ± 0.007	0.562 ± 0.003	0.564 ± 0.008
3	3.394	3.390 ± 0.006	1.337 ± 0.003	1.341 ± 0.008
4	2.887	2.887 ± 0.006	1.844 ± 0.004	1.844 ± 0.008
5	2.845	2.847 ± 0.006	1.886 ± 0.004	1.884 ± 0.008
6	2.262	2.267 ± 0.006	2.469 ± 0.004	2.464 ± 0.008
7	2.167	2.170 ± 0.006	2.564 ± 0.005	2.561 ± 0.008
8	1.324	1.322 ± 0.005	3.407 ± 0.005	3.409 ± 0.008
9	1.143	1.149 ± 0.006	3.588 ± 0.006	3.582 ± 0.009
10	1.104	1.108 ± 0.006	3.627 ± 0.006	3.623 ± 0.009
11	1.083	1.083 ± 0.006	3.648 ± 0.006	3.648 ± 0.009
12	0.989	0.993 ± 0.005	3.742 ± 0.006	3.738 ± 0.008
13	0.890	0.881 ± 0.005	3.841 ± 0.006	3.850 ± 0.008
14	0.825	0.832 ± 0.005	3.906 ± 0.006	3.899 ± 0.008
15	0.802	0.802 ± 0.005	3.929 ± 0.006	3.929 ± 0.008
16	0.544	0.547 ± 0.005	4.187 ± 0.006	4.184 ± 0.008
17	0.529	0.529 ± 0.005	4.202 ± 0.006	4.202 ± 0.008
18	0.506	0.512 ± 0.005	4.225 ± 0.006	4.219 ± 0.008
19	0.178	0.173 ± 0.005	4.563 ± 0.007	4.558 ± 0.009

Table II

The $^{238}U(n,p)^{238}Np$ reaction

Level	Present work ± 0.010	Uncorrected mean	Upper limit to ^{238}Np (Mev)	Corrected mean
	Level (Mev)			
0	0.000	4.723 ± 0.007	0	0
1	0.049	4.859 ± 0.017	0.0471 ± 0.000	0.472 ± 0.008
2	0.109	4.107 ± 0.017	0.062 ± 0.023	0.518 ± 0.008
3	0.394	3.390 ± 0.006	1.137 ± 0.003	1.343 ± 0.008
4	2.007	2.007 ± 0.006	1.381 ± 0.004	1.881 ± 0.008
5	2.845	2.817 ± 0.006	1.006 ± 0.004	1.858 ± 0.008
6	2.262	2.267 ± 0.006	2.409 ± 0.004	2.148 ± 0.008
7	2.147	2.170 ± 0.006	2.584 ± 0.005	2.303 ± 0.008
8	3.324	1.322 ± 0.005	3.407 ± 0.005	3.409 ± 0.008
9	1.143	1.149 ± 0.006	3.598 ± 0.006	3.252 ± 0.009
10	1.104	1.180 ± 0.006	3.687 ± 0.006	3.063 ± 0.009
11	1.043	1.053 ± 0.006	3.868 ± 0.006	3.484 ± 0.009
12	0.969	0.993 ± 0.005	3.748 ± 0.006	3.730 ± 0.008
13	0.890	0.883 ± 0.005	3.841 ± 0.006	3.830 ± 0.008
14	0.825	0.832 ± 0.005	3.906 ± 0.006	3.898 ± 0.008
15	0.802	0.802 ± 0.005	3.929 ± 0.006	3.929 ± 0.008
16	0.544	0.547 ± 0.005	4.187 ± 0.006	4.184 ± 0.008
17	0.529	0.529 ± 0.005	4.202 ± 0.006	4.202 ± 0.008
18	0.506	0.512 ± 0.005	4.225 ± 0.006	4.219 ± 0.008
19	0.174	0.173 ± 0.005	4.563 ± 0.007	4.552 ± 0.009

the other contaminants, since the peak density is so high in this portion of the spectrum.

Errors

The errors quoted in the Q-values and excitation energies are actually a measure of the uncertainties in the measurements of the energy involved. These uncertainties may be separated into two types: one random in nature, and the other systematic. A detailed examination of the uncertainty of each level has not been carried out, but the general effects have been noted, and it is felt that the probable error assigned is a generous estimate of the actual errors.

Q-Value Errors. The factors that may contribute to the random errors are:

1. The spread in energy of the incident particles resulting from finite slit widths;

2. The spread in energy of the emergent particles from variations in target thickness.

3. Failure to keep the fluxmeter pip centered on the oscilloscope.

Now, since each Q-value is the mean of at least two and usually four independent measurements, an estimate of the random error was obtained by calculating the standard error

$$\sigma_{\bar{x}} = \left[\frac{\sum_{1}^{n} (x_i - \bar{x})^2}{n(n-1)} \right]^{\frac{1}{2}}$$

the other contributions, since the peak occurs to an item in this portion of the spectrum.

Errors

The errors caused by the variation and distribution analysis are usually a measure of the uncertainties in the measurements of the energy involved. These uncertainties may be separated into two types: one results in energy, and the other dispersion. A detailed examination of the uncertainty of each level has been carried out, but the general effects have been noted, and it is felt that the observable error involved is a function relative of the actual errors.

Relative errors. The factors that may contribute to the relative errors are:

1. The spread in energy of the incident particles resulting from finite slit widths;

2. The spread in energy of the emergent particles from variations in target thickness.

3. Failure to keep the ionization gap centered on the oscilloscope.

Now, since each value in the range of at least two and usually four independent measurements, an estimate of the relative error was obtained by calculating the standard error

$$\sigma_{\bar{x}} = \left[\frac{\sum_{j}^{n} (x_j - \bar{x})^2}{n(n-1)} \right]^{\frac{1}{2}}$$

where

$\bar{x}$ = mean value of Q for each level

x_i = individual Q-value measurements

n = number of observations.

This procedure resulted in an average value of 2.0 kev for the standard error, and this is taken as an estimate of the random error.

The systematic errors are the more significant ones, and in general they are a function of the energy of the emergent particles. These errors may be due to

1. The calibration error of the magnetic spectrograph, which includes the error in positioning the polonium wire and the uncertainty in the Bρ value of the polonium alpha particles.

2. Uncertainties in determining the one-third height position of the proton peak, and the validity of using the one-third height as a measure of the proton energy. This error also includes the uncertainty in measuring the distance from the strip counted in the microscope to the index mark.

3. Since the energies of the elastically scattered deuterons used for input energy determination and of the protons from the (d,p) reaction are measured after passing through the target, there is an error in the Q-value determination from the difference in energy losses suffered by protons and deuterons. A correction for this effect has been applied to the Q-values, but it is difficult to analyze the effect precisely so that some error is introduced.

where

$\bar{x}$ = mean value of x_j for each level

x_j = individual x-value measurements

n = number of observations.

This procedure resulted in an average value of 2.0 kev for the standard error, and this is taken as the estimate of the random error.

The systematic errors are less clearly defined, and in general they are a function of the energy of the emergent particles. These errors may be due to

1. The calibration error of the magnetic analyzer, which includes the error in positioning the aluminum foils and the uncertainty in the $B\rho$ value of the polarizing field permeable.

2. Uncertainties in determining the cross-sloping backposition of the proton peak, and the validity of using the observed height as a measure of the proton energy. This error also includes the uncertainty in measuring the distance from the origin counted to the microscope to the index mark.

3. Since the energies of the singly-ionized deuterons used for input energy determination and of the protons from the (d,p) reaction are measured after passing through the target, there is an error in the energy determination from the difference in energy losses suffered by protons and deuterons. A correction for this effect has been applied to the results, but it is difficult to analyze the effect precisely as well some error is introduced.

The estimates for each of these errors is given in the following table:

Table III

System Errors in Q-Values

(in percent of proton energy)

1.	Calibration error	0.04
2.	Uncertainty in position of one-third height	0.03
3.	Energy loss in target	0.03

Square root of sum of squares $\approx$ 0.06 percent.

The total error is then taken as the sum of the random and systematic errors. Thus, for the ground state at 30 degrees,

E_p = 11.6 Mev

Random error = 2.0 kev

Systematic error = 6.9 kev

Total error = 9.0 kev.

In order to allow for possible sources of error that may have been overlooked in this analysis, it was decided to list an error of $\pm$ 10 kev for all Q-values.

The particulars for rough of linear errors is given in the following table:

Table III

Errors Errors in Values

(In percent of actual energy)

1. Calibration error	0.05
2. Inhomogeneity in position of non-sliver bolts	0.03
3. Energy loss in target	0.01

Square root of sum of squares = 0.06 percent.

The total error is then taken in the sum of the random and systematic errors. Thus, for the proton stops as 30 degrees,

E_p = 11.3 Mev

Random error = 2.0 Mev

Systematic error = 0.1 Mev

Total error = 2.0 Mev.

In order to allow for possible sources of error that may have been overlooked in this analysis, it was decided to list an error of ± 10 Mev for all D-values.

Excitation Energy Errors. The excitation energy is found by subtracting the Q-value for each level from the ground-state Q-value. The systematic errors in the Q-values then tend to cancel out, particularly for levels corresponding to proton groups which appear on the same plate as those from the ground-state transition. The random error was calculated as for the Q-values by examination of the standard errors of the mean value and was again found to be about 2 kev. The systematic error was taken as 0.1 percent of the excitation energy.

Deflection Energy Errors. The excitation energy is found by subtracting the Q-value for each level from the ground-state Q-value. The systematic error in the previous item had to cancel out, particularly for levels corresponding to broken groups which appear on the same plate as those from the ground-state transition. The random error was calculated as for the Q-values by combination of the standard errors of the mean value and one again found to be about 2 kev. The systematic error was taken as 0.3 percent of the excitation energy.

V. Conclusions

The present investigation of the $P^{31}(d,p)P^{32}$ reaction using the broad-range spectrograph has extended the information on the energy levels of P^{32} up to 4.56-Mev excitation. In addition, several levels that were missed in previous investigations have been observed. The existence of the low-lying state at an energy of 77 kev has been confirmed. This state can be explained as arising from the two different orientations of the unpaired s-proton hole relative to the angular momentum of the unpaired d-neutron. The very small splitting observed requires a comparatively weak spin exchange force even though the two particles, being in different orbital states, do not interact strongly. Because the lowest states would be those with parallel spins, the ground state of P^{32} should have spin 1 and the excited states, spin 2. The states in question are members of spin doublets, and the dependence of their reaction cross section on the spin J_B of the residual nucleus is predicted by stripping theory.

In the stripping theory developed by Butler[3], the only term in the cross-section formula that depends on the spin of the final nucleus is $(2J_B + 1)$. We can thus use the intensities of the proton groups corresponding to the two levels to check on the spin assignments made from stripping theory; $J_B = 1$ for the ground state and $J_B = 2$ for the 77-kev level. These values lead to a predicted ratio

5. Conclusions

$$\frac{(2J_B + 1)_1}{(2J_B + 1)_0} = \frac{5}{3} = 1.67.$$

The ratios of intensities found in this experiment were 30°:1.61; 50°:1.52; 70°:1.44; and 90°:1.41 for an average of 1.5 so that at least qualitative agreement is evidenced.

This investigation served to demonstrate that an accurate analysis of energy levels can be made in the presence of a relatively large number of contaminant nuclei, provided the masses of the contaminants are not too close to the mass of the nucleus being studied. This ability becomes increasingly important as more nuclei are investigated which must be used in compound form to facilitate vacuum evaporation of the material onto the Formvar backings.

$$\frac{(2h_3^3 + 1)_1}{(2h_3^3 + 1)_3} = \frac{\xi}{\gamma} = 1.67.$$

The ratios of independent terms in these experiments were 30^0:1.61; 50^0:1.39; 70^0:1.44; and 90^0:1.61 for an average of 1.5 as that at least qualitative agreement is evidenced.

This investigation served to demonstrate that an accurate analysis of energy levels can be made in the presence of a relatively large number of contaminant ions, provided the lines of the contaminants are not too close to the lines of the nuclei being studied. This ability becomes increasingly important as more nuclei are investigated which must be used in compound form to facilitate vapor evaporation of the material onto the Varian backing.

BIBLIOGRAPHY

1. M. G. Mayer and J. H. D. Jensen, Elementary Theory of Nuclear Shell Structure, John Wiley and Sons, Inc. New York (1955)
2. S. Goldstein and I. Talmi, Phys. Rev. 105, 995 (1957)
3. S. T. Butler and O. H. Kittmair, Nuclear Stripping Reactions, John Wiley and Sons, Inc, New York (1957)
4. R. Huby, PROGRESS IN NUCLEAR PHYSICS, edited by O. R. Frisch, Vol. 3, Sec. 7, Pergamon Press, Ltd, London, (1953)
5. Buechner, Sperduto, Browne, and Bockelman, Phys. Rev. 91, 1502 (1953).
6. C. P. Browne and W. W. Buechner, Rev. Sci. Instr. 27, 899 (1956).
7. W. W. Buechner, PROGRESS IN NUCLEAR PHYSICS, edited by O. R. Frisch, Vol. 5, Sec. 1, Pergamon Press, Ltd, London (1956)
8. Buechner, Strait, Sperduto, and Malm, Phys. Rev. 76, 1543 (1949)
9. R. D. Evans, THE ATOMIC NUCLEUS, McGraw-Hill Book Company, Inc. New York (1955)
10. Enge, Wahlig, and Aanderaa, Rev. Sci. Instr. 28, 145 (1957)
11. H. A. Enge, Ph. D. Thesis, Universitetet i Bergen, Norway (1954)
12. H. A. Enge, Rev. Sci. Instr. 23, 599 (1952)
13. Van Patter, Endt, Sperduto, and Buechner, Phys. Rev. 86, 502 (1952)
14. Dalton, Hinds, and Parry, Proc. Phys. Soc. 70A, 586 (1957)
15. A. Sperduto and W. W. Buechner, Phys. Rev. 88, 574 (1952).

1. M. O. Dayer and J. H. D. Jensen, Elementary Theory of Nuclear Shell Structure, John Wiley and Sons, Inc. New York (1955)

2. S. Goldstein and I. Tamm, Phys. Rev. 105, 955 (1957)

3. T. Watabe and O. H. Hattori, Nuclear Structure Lectures, Asia Wiley and Sons, Inc, New York (1957)

4. J. Rudy, PROCEEDINGS IN NUCLEAR PHYSICS, edited by O. L. Friedy, Vol. 5, Sec. 7, Pergamon Press, Ltd, London, (1953)

5. Bowsher, Spreyfuto, Proces, and Nolsinkum, Phys. Rev. 91, 1502 (1953).

6. O. P. Breuse and W. H. Bweimer, Rev. Mod. Inter. 27, 599 (1956).

7. W. W. Hwaslum, PROGRESS IN NUCLEAR PHYSICS, edited by O. H. Friedy, Vol. 5, Ann. L, Pergamon Press, Ltd, London (1954)

8. Hwaslum, Hurst, Spreyfuto, and Wolny, Phys. Rev. 76, 1813 (1949)

9. L. D. Swaze, THE ATOMIC NUCLEUS, McGraw-Hill Book Company, Inc. New York (1955)

10. Swye, Wolfit, and Asterra, Rev. Mod. Inter. 28, 316 (1957)

11. H. A. Swye, Ma. D. Theeis, Lectures-Notes I Swyes, Norway (1958)

12. H. A. Swye, Ann. Phil. Chem. 63, 599 (1956)

13. Van Pasker, Swift, Spreyfuto, and Hwaslum, Phys. Rev. 86, 502 (1952)

14. Swiss, Wilde, and Swift, Proc. Phys. Soc. 70A, 814 (1957)

15. A. Spreyfuto and W. H. Bweimer, Phys. Rev. 83, 571 (1952).